Interaction between rarefaction wave and viscous fingering in a Langmuir adsorbed solute

Chinar Rana and Manoranjan Mishra*
Department of Mathematics, Indian Institute of Technology Ropar, 140001 Rupnagar, Punjab, India

(Received 2 April 2019; revised manuscript received 4 January 2020; accepted 3 February 2020; published 2 March 2020)

The evolution of dissolved species in a porous medium is determined by its adsorption on the porous matrix through the classical advection-diffusion processes. The extent to which the adsorption affects the solute propagation in applications related to chromatography and contaminant transport is largely dependent upon the adsorption isotherm. Here, we examine the influence of a nonlinear Langmuir adsorbed solute on its propagation dynamics. Interfacial deformations can also be induced by classical viscous fingering (VF) instability that develops when a less viscous fluid displaces a more viscous one. We present numerical simulations of an initially step-up concentration profile of the solute that capture a rarefaction/diffusive wave solution due to the nonlinearity introduced through Langmuir adsorption and variety of pattern-forming behaviors of the solute dissolved in the displaced fluid. The fluid velocity is governed by Darcy's law, coupled with the advection-diffusion equation that determines the evolution of the solute concentration controlling the viscosity of the fluids. Numerical simulations are performed using the Fourier pseudospectral method to investigate and illustrate the role played by VF and Langmuir adsorption in the development of the patterns of the interface. We show that the solute transport proceeds by the formation of a rarefaction wave results in the enhanced spreading of the solute. Interestingly we obtained a nonmonotonic behavior in the onset of VF, which depends on the adsorption parameters and existence of an optimal value of such adsorption constant is obtained near $b = 1$, for which the most delayed VF is observed. Hence, it can be concluded that the rarefaction wave formation stands out to be an effective tool for controlling the VF dynamics.

DOI: 10.1103/PhysRevE.101.033101

I. INTRODUCTION

Despite the range of significant applications of solute transport in a porous medium, including improved oil recovery [1], contaminant transport [2,3], and CO_2 sequestration [4], the long-term fate of nuclear waste repositories, secure storage of carbon dioxide, the qualitative behavior of the contaminant mixing in the soil-water system, remain uncertain [5]. The experiments on separation columns [6], field studies on soil-water contamination [2] have shown that the transport is characterized by the early breakthrough of the solute, tailing of the concentration at later times and in many cases virtually immobile peak concentration [7]. Thus, transport cannot be described by a traditional advection-dispersion formulation only; instead, other theories, including the interaction of the solute with the porous medium via adsorption [8], nonconventional stresses at the interface [9], or reaction between the components [10,11], have been employed to describe the evolution of dissolved species over time. There have been various studies on the adsorption phenomena in the porous medium related to applications in enhanced oil recovery, CO_2 capture, and contaminant transport [3,12–14]. There have been linear and nonlinear equilibrium models developed to describe the adsorption kinetics [15]. However, the understanding of adsorption effects on the transport of the solute is scant partially because of the limited experimental data and computationally challenging because of the complexity introduced by a nonlinear adsorption isotherms and they are of several types depending on the adsorbent and adsorbate (e.g., Langmuir Isotherm, Freundlich Isotherm, Toth Isotherm, Langmuir-Freundlich Isotherm, etc.) [6,16–18]. In view of this, we devote this article to the computational study of the transport behavior of the solute undergoing nonlinear adsorption of Langmuir type, defined as

$$c_s = \frac{K c_m}{(1 + b c_m)}, \tag{1}$$

where c_s and c_m are the stationary and mobile phase solute concentrations, K is the equilibrium constant, and b is the nonlinear adsorption parameter.

For the nonlinear adsorption of Langmuir type, the pioneering work of De Vault (1943) [19] showed that if the initial concentration increases along the direction of flow, it results in a highly dispersed concentration profile which otherwise is self-sharpening for decreasing initial concentration. The self-sharpening wavefront is called shock wave in the ideal case and a shock layer when accompanied by diffusion. Whereas, the nonsharpening wave fronts tend to attain a proportionate pattern called a rarefaction wave [8]. The formation of these nonlinear waves is because of the fact that the Langmuir adsorption results in the advection and the dispersion rate of the solute to be a function of the concentration [12]. Edström *et al.* [20] have demonstrated experimentally the influence of

*manoranjan@iitrpr.ac.in

Langmuir adsorption on the deformation of the peak shape of the solute in a reverse phase chromatography column (RPLC). In an application related to flow of polymers with retention depending upon the solute concentration (as in the case of Langmuir adsorption), Dominguez *et al.* [21] have performed experiments to illustrate the solute peak shapes showing occurrence of highly diffused and sharpened concentration profiles. There have been theoretical studies on the influence of Langmuir adsorption on the shock wave front properties which infer that self-sharpening effect is enhanced with the increase in retention of the solute in the porous matrix [22–24]. However, as per our knowledge, there has not been a single theoretical study reported on the influence of nonlinear adsorption on the rarefaction wave front spreading, which is the main objective of the present model.

Nevertheless, in processes like chromatography [25], CO_2 sequestration [26], and groundwater contamination [27], the viscosity difference between the interplaying fluids play a significant role. Variations in the viscosities of the solutions flowing in porous media may result in the development of an instability at the solution interface [28]. The instability manifests itself in the form of finger-shaped intrusions of the less viscous fluid solution into the more viscous one and referred to as viscous fingering instability [29]. Thus, in addition to the interaction of the fluids with the porous matrix via adsorption, viscous fingering comes into play too. The Langmuir adsorption coupled with the viscosity contrast between the displacing and displaced fluid makes the model more complex to solve. There have already been various studies on the influence of the viscous fingering on a linearly adsorbed solute. In this regard, the experimental results considering these two effects have clearly shown that the adsorption reduces the effect of VF on the solute propagation [30] and theoretically have been verified by Mishra *et al.* [31]. The study of the influence of retention of the solute on the fingering dynamics is carried out in different scenarios for instance linearly adsorbed solute passively following sample solvent [32] or with variable retention inside the sample solvent [33–35].

Zhou *et al.* [36] recently reported that polymer flooding is very effective for enhanced heavy oil recovery methods. The polymer flooding process involves the injection of polymer-water solutions followed by water injection that results into the miscible VF interface of the water and polymer-thickened-water due to the existence of viscosity gradient between them. Also, it is well known that the polymer can adsorb into the porous matrix following the Langmuir isotherm [37,38]. Since it has higher concentration than the water, a rarefaction wave solution can be formed and existence of such solutions is well reported in the literature of enhanced oil recovery processes [39]. In another application of preparative scale size exclusion chromatography the solution of high molecular weight polymers are more viscous and with higher concentration than the mobile phase. The sample mixture does not dilute during the elution. In these processes VF significantly affects the peak shapes [40]. Also, in the cases of high molecular protein separation or in supercritical fluid chromatography, it is clearly observed that the adsorption isotherm of the solute/analyte on the porous bed affects the peak profiles [41,42]. Since the concentration profile is a step-up type the experimental observation of Enmark *et al.* [42] clearly shown a tailing phenomena of the peak shape and it is known as a diffusive wave in the chromatography literature. This nonlinear wave type is known as rarefaction wave in the other porous media applications, e.g., chemical enhanced oil recovery and contaminant transport processes, the detail about such phenomena in porous media applications are explained by Sheng [17], Berkowitz *et al.* [16], Allen III *et al.* [43], and in several other articles in chromatography literature [12,44,45].

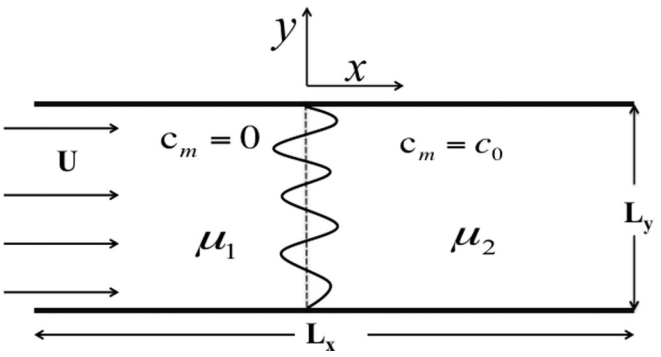

FIG. 1. Schematic of the system.

Recently, Rana *et al.* [22] have analyzed the influence of VF and the shock layer wave front of the solute undergoing Langmuir adsorption. The results show significant change in spatiotemporal behavior of the solute dynamics, which, depending on the values of the adsorption parameters results in an earlier onset of instability and vanishing of the shock layer. Further, Rana *et al.* [46,47] studied the effects of Langmuir and anti-Langmuir adsorption on the band broadening for a finite width sample and investigated the interaction of both nonlinear waves and its influence on VF dynamics, in which one interface was with rarefaction wave and other one with shock layer. However, the influence of VF on the rarefaction wave solution on the semi-infinite interface is yet to be understood, as this could be useful to analyze the frontal dynamics of chromatographic separation applications as explained earlier as well as oil recovery and contaminant transport processes where control of VF is crucial for the output of the process. In the present study, we examine the influence of VF and rarefaction wave front formed due to Langmuir adsorption, on the transport dynamics of the solute. Our numerical simulation results have been able to provide insights into the effect of the adsorption parameters on the spreading of the rarefaction wave and further its influence on the onset of VF instability. We have found an optimal adsorption parameter b for having the most delayed onset of VF for different log mobility ratio R. Recently, different techniques have been investigated to control the VF instability [48,49] and we observe that the rarefaction wave formation stands out to be an effective tool.

II. MATHEMATICAL MODEL

The setup we considered is depicted in Fig. 1. The flow is in the longitudinal direction, where a fluid of viscosity μ_1 with $c_m = 0$ is displacing a fluid of viscosity μ_2 ($>\mu_1$) with $c_m = c_0$. In the moving reference frame, moving with

injection velocity U, the nondimensional governing equations for two-dimensional displacement of the concentration in a miscible, incompressible fluid system are [46]

$$\underline{\nabla} \cdot \underline{u} = 0, \tag{2}$$

$$\underline{\nabla} p = -\mu(c_m)(\underline{u} + \underline{e_x}), \tag{3}$$

$$\left(1 + \frac{k}{(1+bc_m)^2}\right)\frac{\partial c_m}{\partial t} - \frac{k}{(1+bc_m)^2}\frac{\partial c_m}{\partial x} + \underline{u} \cdot \underline{\nabla} c_m = \frac{\partial^2 c_m}{\partial x^2} + \frac{\partial^2 c_m}{\partial y^2}. \tag{4}$$

Here $\underline{e_x}$ is unit vector in axial direction, $\underline{u} = (u, v)$ is the velocity field, p is the pressure, k is the retention parameter, and $\mu(c_m)$ is the viscosity of the fluid depending on the mobile phase solute concentration as

$$\mu(c_m) = e^{Rc_m}, \tag{5}$$

where $R = \ln(\mu_2/\mu_1)$ is the log-mobility ratio. With $\mu_1 < \mu_2$, $R > 0$, hence the flow is unstable resulting in VF instability. However, with $\mu_1 \geqslant \mu_2$, i.e., for $R \leqslant 0$, the proposed model shows a stable displacement [50].

A. Initial and Boundary conditions

The initial condition ($t = 0$) for mobile phase solute concentration c_m is

$$c_m(x, y) = \begin{cases} 0, & \text{for } x < 0 \\ 1, & \text{for } x \geqslant 0 \end{cases} \quad \forall y. \tag{6}$$

The boundary conditions are

$$(u, v) = (1, 0), \quad \frac{\partial c_m}{\partial x} = 0 \ \forall y \text{ as } |x| \to \infty, \tag{7}$$

$$\frac{\partial v}{\partial y} = 0, \quad \frac{\partial c_m}{\partial y} = 0, \quad \forall x \text{ at the transverse boundaries.} \tag{8}$$

The analytical solution of the unidimensional solute transport equation in the ideal case exists and the characteristic solution with step-up initial solute concentration shows formation of expanding waves (for details, see the Appendix). However, to understand the overall dynamics of the adsorbed solute, a full nonlinear set of equations [Eqs. (2)–(4)] needs to be solved numerically. In what follows, a brief description of the numerical simulation technique to handle the full nonlinear problem is followed by discussion of the results obtained for stable and unstable displacements.

B. Numerical analysis

The nonlinear dynamics of the concentration $c_m(x, y)$ for the proposed model are examined in a computational domain of size $L \times L'$. Using stream function $\psi(x, y)$ as $(u, v) = (\partial\psi/\partial y, -\partial\psi/\partial x)$, the governing Eqs. (2)–(4), after applying the stream function-vorticity formulation and using Eq. (5), become

$$\nabla^2 \psi = -\omega, \tag{9}$$

$$\omega = R\left(\frac{\partial \psi}{\partial x}\frac{\partial c_m}{\partial x} + \frac{\partial \psi}{\partial y}\frac{\partial c_m}{\partial y} + \frac{\partial c_m}{\partial y}\right), \tag{10}$$

$$\left(1 + \frac{k}{(1+bc_m)^2}\right)\frac{\partial c_m}{\partial t} - \frac{k}{(1+bc_m)^2}\frac{\partial c_m}{\partial x} + \frac{\partial \psi}{\partial y}\frac{\partial c_m}{\partial x} - \frac{\partial \psi}{\partial x}\frac{\partial c_m}{\partial y} = \frac{\partial^2 c_m}{\partial x^2} + \frac{\partial^2 c_m}{\partial y^2}. \tag{11}$$

The above set of governing Eqs. (9)–(11) are solved by using Fourier-pseudo spectral method [51], which requires periodic boundary conditions (for details, cf. Ref. [22]). In the proposed problem periodicity can be applied in the transverse direction, without loss of generality. However, in the longitudinal direction, the periodic extension of the concentration on the right of the computational domain is included [52,53]. A resolution of 2048×256 is used throughout this study with a time step of $dt = 0.2$ and spatial step size of $dx = dy = 4$. In numerical scheme the initial condition of step-up mobile phase concentration is implemented by setting $c_m = 0$ and $c_m = 1$ with an intermediate value as $1/2 - Ar$, where r is random number between 0 and 1 and A is the amplitude of noise of order 10^{-3}. We start our analysis in Sec. III by examining the influence of Langmuir adsorption on the concentration when there is no viscosity difference between the interplaying fluids ($R = 0$). Next, in Sec. IV the influence of viscous fingering ($R \neq 0$) on the concentration $c_m(x, y)$ is discussed. The parameter values are so chosen, that the dynamics of the concentration under the effect of Langmuir adsorption is apparent.

III. NONLINEAR DYNAMICS: VISCOUSLY STABLE

In Fig. 2 the propagation dynamics of the mobile phase solute concentration is shown for linear ($b = 0$) and Langmuir ($b = 5$) adsorption configuration with $R = 0$, i.e., both the displacing and displaced fluids having the same viscosity. In Fig. 2(a) the initial mobile phase concentration is shown, where the red color depicts $c_m = 0$ and blue color depicts $c_m = 1$. Since simulations are performed in a moving frame of reference, the miscible interface moves in the upstream direction. For $b = 0$, Fig. 2(b) shows pure diffusing profiles, whereas for $b = 5$ [Fig. 2(c)] the miscible interface is highly diffused.

In the following we explain the choice of the adsorption parameters k and b in our simulations. The Langmuir adsorption constant b is an empirical constant, in dimensional form of $\hat{b}$, the unit is the reciprocal of the unit of saturation solute concentration c_{sat}, i.e., $\hat{b} = K/c_{\text{sat}}$, where K is the equilibrium constant and $k = FK$, where F is the phase ratio volume of solute in the stationary and mobile phases, the detail explanations are given in Rana *et al.* [46]. If $b = 0$, then the adsorption becomes linear; for $b < 0$ adsorption is unfavorable and for $0 < b < \infty$ adsorption is favorable [18]. In the experiments, the Langmuir constant b are chosen to fit the data for finding the isotherms with different mobile phases and they are found to vary from $O(10^{-1})$ to $O(10^3)$ [17,54]. Ali and Ben Mahmud [55] performed an experiment for adsorption of hydrolyzed polyacrylamide (HPAM) polymer on standstone surface and found that such Langmuir constants can depend on the salinity and varies from 9.64 to 29.67 L/g in dimensional scale corresponding to the increasing of salinity from 0 to 4 wt %. Recently, in an oil recovery

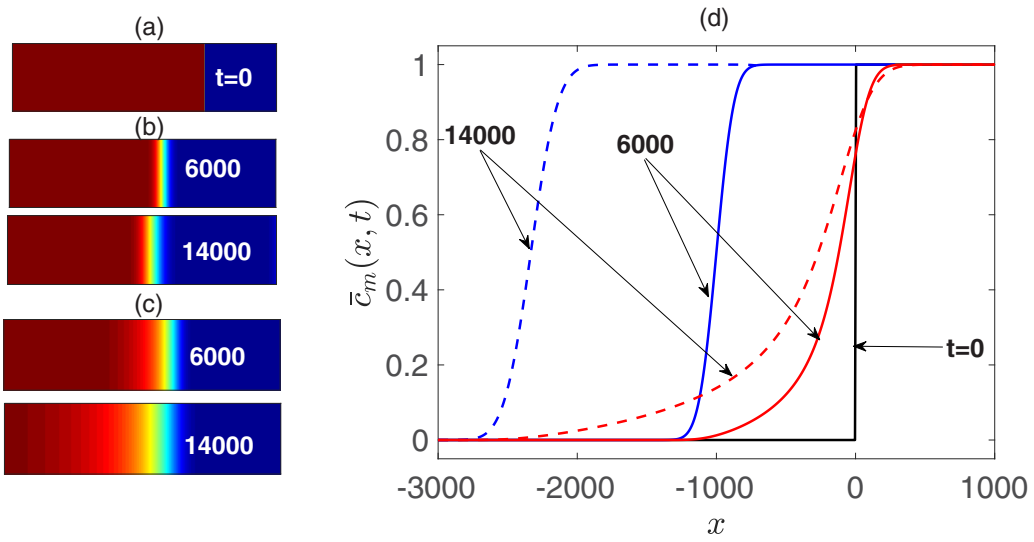

FIG. 2. (a–c) Concentration fields $c_m(x, y)$ with $R = 0, k = 0.2$, (a) initial concentration at $t = 0$, (b) for $b = 0$ (Linear adsorption), and (c) $b = 5$ (Langmuir adsorption). (d) The corresponding transversely averaged concentration profiles $\bar{c}_m(x, t)$ for $b = 0$ (blue lines), error function solutions away from the step-up curve at $t = 0$ and $b = 5$ (red lines), rarefaction solutions where the part of the curve with higher concentrations are near to the step-up curve at $t = 0$.

problem Falode and Afolabi [56] have considered the adsorption constant k as 6.5, 13.5, 20 for different clay mineral Kaolinite, Illite, and Montmorillonite, respectively, and the constant b as 100. Therefore, we conclude that considering the constant $b > 0$ and upto a $O(10^2)$ is sufficient enough to study the effects of the Langmuir adsorption and we show in the following that when $b \to 100$, the VF dynamics reach to an asymptotic spreading.

To better understand the propagation dynamics of the concentration, the transversely averaged concentration profile of $c_m(x, y)$ is calculated as [57]

$$\bar{c}_m(x,t) = \frac{1}{L'}\int_0^{L'} c_m(x,y,t)dy$$

and is plotted in Fig. 2(d). The average profile $\bar{c}_m(x, t)$ for $b = 0$ depicts the error function solution, however, for Langmuir adsorption with $b = 5$, the concentration profile forms a highly stretched wave called as rarefaction wave [see Fig. 2(d)]. The experiments performed by Dominguez *et al.* [21] and Edstörm *et al.* [20] have shown the occurrence of such highly diffused fronts of the retained solute in applications related to polymer transport and chromatography (see Figs. 3 and 4 in Ref. [21] and Fig. 3 in Ref. [20]). Thus, these experimental results are in good comparison with our theoretical model.

This significant change in the dispersive regime of the Langmuir adsorbed solute is due to the variation in advection and dispersion rates with solute concentration c_m. The axial propagating velocity of the Langmuir adsorbed solute in the upstream direction is $k/[k + (1 + bc_m)^2]$ [can be deduced from Eq. (11)], whereas the linear adsorbed solute ($b = 0$) propagates with $k/(1 + k)$ velocity. The dependence of the advection speed of the solute on its concentration c_m results in changing the propagation dynamics of the solute. It is clearly observed that for $b \neq 0$ advection speed decreases with an increase in c_m. Hence, in comparison to higher concentration the lower concentrations are advecting faster in the upstream direction, which leads to the formation of an expanding wave. Further, it is essential to analyze the influence of the Langmuir adsorption on the dispersion rate of the concentration. From Eq. (11), the dispersion rate is obtained as $[(1 + bc_m)^2]/[k + (1 + bc_m)^2]$. It is observed that for $b \neq 0$ dispersion rate increases with increase in average concentration $\bar{c}_m$. Therefore, the low concentration regions are advecting more and dispersing less, whereas high concentration regions show an opposite trend. This scenario is clearly observed in Fig. 2(b) (dashed red lines), where higher concentrations are dispersed more and less advected in comparison to the lower ones. The experimental profiles for the supercritical fluid chromatography by Enmark *et al.* [42] shows the formation of stretched waves for the Langmuir adsorbed solute and thus are in good agreement with our numerical results.

A. Effects of adsorption parameter *b*

To understand the effect of increasing value b on the dispersive regime of the miscible interface, the concentration $c_m(x, y)$ for different values of b are shown in Fig. 3. The interfacial concentration profiles show the dispersive region of the solute first increasing with b [see Fig. 3(a) for $b = 0.1, 1$] and then decreasing (for $b = 10$). Thus, the spreading of the solute concentration is varying nonmonotonically with b. In Fig. 3(b) the corresponding averaged concentrations, $\bar{c}_m(x, t)$ are shown for different values of b at a fixed time $t = 10^4$. For $b \leqslant 1$ the concentration profiles are observed to be expanding with b, but with a compression toward the lower concentration zone for $b > 1$. The dependence of the advection and dispersion rate on the concentration and adsorption parameter b, leads to such dynamics. Since the advection rate decreases with increase in b the concentration profile shown in Fig. 3(b) shows the front for larger b to be least advected in the upstream direction. Furthermore, as the dispersion rate increases with increase in b, therefore the concentration

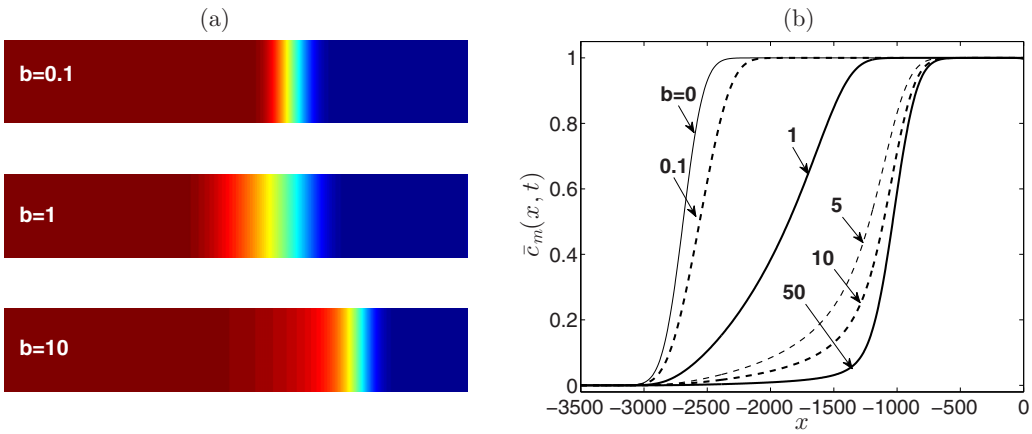

FIG. 3. (a) The mobile phase solute concentration $c_m(x, y)$ fields with $R = 0,\ k = 0.2$ for different values of b at a fixed time $t = 10^4$. (b) The corresponding transversely averaged concentration profile $\bar{c}_m(x, t)$.

profiles shown in Fig. 3(b) is more dispersed for larger values of b in comparison to lower values of b. Moreover, since the advection and dispersion are also functions of concentration hence, as described in the previous section, the spreading is varying with the concentration as well. In order to analyze the effect of b on the spreading of the solute we quantify the spreading length in the next section

B. Evolution of the spreading length

The quantification of the spreading length, L_m, of $\bar{c}_m(x, t)$ is a good measure to analyze the influence of b. The spreading length is quantified as the length of the interval in which $0.001 < \bar{c}_m(x, t) < 0.999$. The spreading length L_m is shown in inset Fig. 4 for different values of b with $k = 0.2,\ R = 0$. It is observed that L_m increases with increase in b, but decreases eventually for $b > 20$. In Fig. 4 we plotted L_m as a function of b, at a fixed time $t = 10^4$. It is observed that the increment in L_m is more for smaller b, however, as b increases the increment reduces and then eventually decreases.

The spreading length results are anti-synergetic, because the rarefaction wave front formed due to Langmuir adsorption

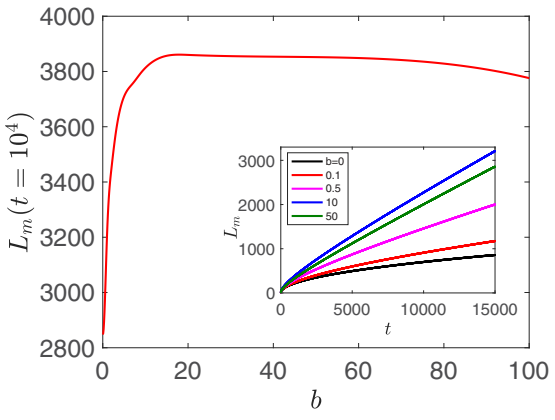

FIG. 4. The spreading length L_m as a function of b at a fixed time $t = 10^4$. Inset: Evolution of the spreading length L_m for different values of b (from below $b = 0,\ 0.1,\ 0.5,\ 50$, and 10), with $R = 0,\ k = 0.2$.

is expected to always expand the concentration profile. Since, the solute spreading occurs because of the influence of the advection and dispersion, to explain the counterintuitive result of nonmonotonicity in the spreading dynamics, we again take a close inspection of the two scenarios, advection and dispersion rate. It is observed that the dispersion rate increases with b but the advection speed decreases. Thus, the spreading of the concentration for large b, is due to dispersion only, whereas for small b the advection rate is the main cause of spreading. Hence, a threshold is reached at $b \simeq 20$, where L_m starts decreasing. This is due to the fact that for sufficiently large values of b, here $b = 20$, the axial advection speed reduces significantly [advection speed $= k/[k + (1 + bc_m)^2]$], which results in decrease in spreading of the solute. Moreover, as $b \to \infty$ the solute transport equation approaches no-adsorption case which depicts solute spreading $\propto t^{1/2}$ [57].

IV. NONLINEAR DYNAMICS: VISCOUS FINGERING EFFECTS

In applications related to chromatography, enhanced oil recovery, CO_2 sequestration, the mobility gradients developed due to the variation in the viscosity of the interplaying fluids results in the occurrence of viscous fingering instability that significantly changes the solute propagation [52]. Our aim is to investigate the influence of rarefaction wave on the occurrence of VF instability and thus to use it as a tool to manipulate the instability dynamics.

A. Influence of adsorption parameter *b*

To investigate the influence of Langmuir adsorption on the viscous fingering dynamics, the log mobility ratio is chosen as $R = 1$. The concentration density profiles, $c_m(x, y)$, depicting the fingering dynamics with $R = 1$ for different values of b are plotted in Fig. 5. It is clearly observed that fingering dynamics in the Langmuir adsorbed solute ($b \neq 0$) is quite different from the linearly adsorbed solute ($b = 0$). For $b = 1$ [Fig. 5(b)], the concentration fields show delay in formation of fingers in comparison to $b = 0$ [Fig. 5(a)]. As already explained in Fig. 3, the Langmuir adsorption leads to expansion of the concentration front. This spreading results

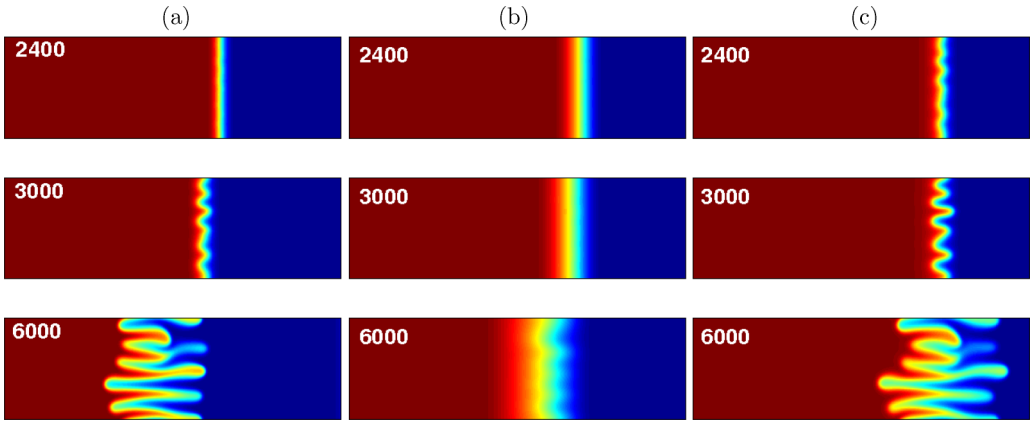

FIG. 5. The concentration plots for $R = 1$, $k = 0.2$ and (a) $b = 0$, (b) $b = 1$, (c) $b = 50$.

in decreasing the concentration gradient across the miscible interface between the displaced and displacing fluids. As a consequence, the effective viscosity gradient decreases along the interface, which leads to delay in the onset of VF. Hence, the fingering pattern can be observed to be delayed for $b = 1$ in comparison to $b = 0$. Thus, the presence of the rarefaction wave can weaken the finger formation. However, for $b = 50$ [Fig. 5(c)], contrasting dynamics in the form of sharp fingers are observed, which appear early in comparison to $b = 1$. For $b = 0$ the onset of fingering is around $t = 3000$ [Fig. 5(a)]. However, as stated earlier onset is observed to delay for $b = 1$, showing fingering pattern at $t = 6000$ [Fig. 5(b)].

However, for $b = 50$ the fingering dynamics are observed early at time $t = 2400$, whereas at this time $b = 0$ shows no fingering pattern. Thus, viscous fingering dynamics are observed earlier for large b in comparison to $b = 0$. This is because, the concentration is compressed for large values of b (>10) (see Fig. 4) thus resulting in creating a higher concentration gradient along the miscible interface which favors the viscous fingering instability. Moreover, for $b \to \infty$ Eq. (11) reduces to the case of no-adsorption and for $b = 0$ it reduces to linear adsorption. Thus, from Mishra *et al.* [58], the onset for linear adsorption is delayed by $1/(1 + k)$ times the onset for no-adsorption case. Therefore, in our case for $b = 50$ the onset of VF is observed earlier in comparison to $b = 0$. Hence, the instability can be manipulated (delayed or early) by controlling the nonlinear adsorption parameter b. To compare the dynamics of the concentration for different values of b at a fixed time, the concentration contours for $c_m = 0.17,\ 0.34,\ 0.51,\ 0.68$, and 0.85 are shown in Fig. 6 for different values of b at a fixed time $t = 4000$ for $R = 1$ and $k = 0.2$. The change in fingering dynamics with b can be clearly understood from this figure. For $b = 0$, rigorous fingering dynamics are seen in the concentration contours. However, with $b \neq 0$ the fingers are suppressed because of the rarefaction wave formation. But, again strong fingers are seen for $b = 5$ in comparison to $b = 1$.

B. Transversely averaged concentration profiles

Another significant dynamic change is that, with Langmuir adsorption the concentration front is not distorted symmetrically by the fingers, unlike the case of $b = 0$. The transversely averaged concentration profile $\bar{c}_m(x, t)$ plotted in Fig. 7 for $b = 1$ and $b = 5$ with $R = 1$ clearly shows the difference in the distortions at the interface. In Fig. 7(a) the concentration profile shows distortions toward the higher concentration region. While for $b = 5$ [Fig. 7(b)] the interface is distorted toward both high and low concentrations. For $b = 1$ the fingers are unable to intrude much in the low concentration zone and are propagating mostly toward the higher concentration zone. However, these dynamics of the fingering pattern disappear for $b > 1$, for instance for $b = 5$, the fingers in the dispersive zone intrude both toward high as well as low concentration zones. The evolution profiles obtained by Enmark *et al.* [42] for the Langmuir adsorbed solute with the viscous fingering instability matches well with the instability profile obtained by our numerical simulations.

To explain this interesting dynamic of change in the distortion pattern at the interface with b, we trace the concentration $\bar{c}_m(x, t)$ corresponding to the inflection point for $R = 0$. Since the inflection point refers to the value of x, where the concentration $\bar{c}_m(x, t)$ changes slope from increasing to decreasing

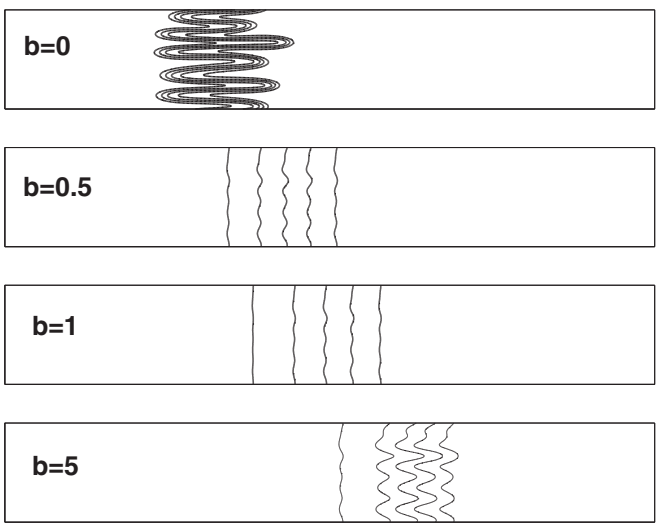

FIG. 6. The contour plots of the concentration at fixed $t = 4000$, for $R = 1$, $k = 0.2$ for different values of b, showing nonmonotonicity in the fingering pattern. The contour lines correspond to $c_m = 0.17,\ 0.34,\ 0.51,\ 0.68$, and 0.85.

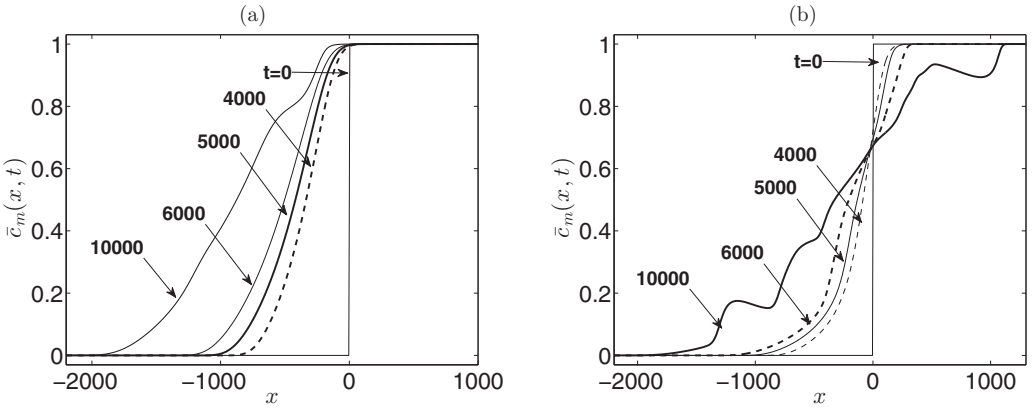

FIG. 7. The transversely average concentration profile $\bar{c}_m(x,t)$ with $R=1$, $k=0.2$ for (a) $b=1$, (b) $b=5$.

and thus is obtained as a peak in the spatial evolution of $d\bar{c}_m/dx$. The concentration corresponding to the inflection point is referred as c_{m_i}, whose evolution with time gives a view about the change of the value of the concentration when its gradient is large. In Fig. 8, c_{m_i} is plotted as a function of time for different values of b. It shows that for $b=0$, the inflection point always lay near the mid value of concentration and it does not evolve with time. However, for $0<b\leqslant 1$ a sudden shift of the inflection point toward the higher concentration is observed. As a consequence, for $b=0$ a higher concentration gradient always lies toward the mean value of the concentration. Thus, for linear adsorption, as soon as there is viscosity contrast between the interplaying fluids, i.e., $R>0$, the fingers are able to easily intrude toward both the high and low concentration zones. Whereas, for $b\neq 0$ high concentration gradient is toward the larger values of c_m that gives rise to the existence of a higher viscosity gradient at that location. Hence, in Langmuir adsorption fingers are able to intrude in the higher concentration zone only. This scenario can be clearly observed from Fig. 7(a). However, for $b>1$ the inflection points again revert back to the mean value of the concentration. This implies that a higher concentration gradient again moves back toward the mean value of the concentration. Thus, resulting in the existence of a higher viscosity gradient at the corresponding location. Hence, fingers intrude toward both the high and low concentration zones [see Fig. 7(b)]. The analysis of the influence of Langmuir adsorption parameter b on the onset time of VF is discussed in the following section.

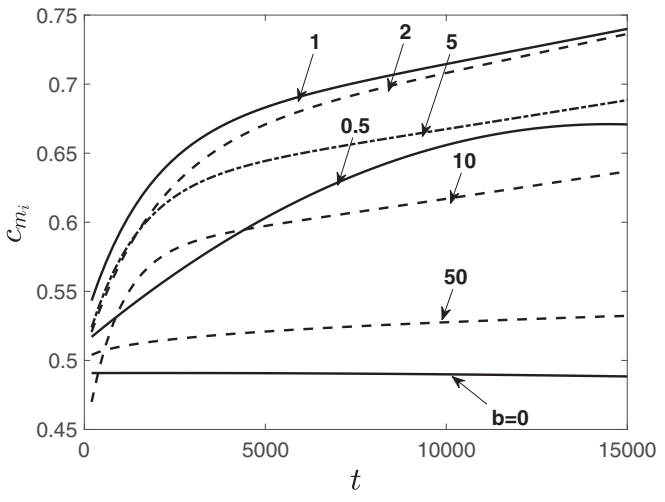

FIG. 8. The temporal evolution of concentration corresponding to the inflexion point, c_{m_i} for different values of b with $R=0$, $k=0.2$.

C. Onset time of fingering

To evaluate the onset time of VF $t_{\rm vf}$, we compute the interfacial length, $I(t)$, which measures the temporal variation of the axial and transverse gradients of the concentration. It is defined as [59]

$$I(t)=\int_0^{L'}\int_0^{L}\left(\frac{\partial c_m}{\partial x}\right)^2+\left(\frac{\partial c_m}{\partial y}\right)^2 dxdy. \tag{12}$$

$I(t)$ is plotted in Fig. 9(a) for $R=1$, $k=0.2$ for different values of b. The onset time $t_{\rm vf}$ is defined as when $I(t)$ increases by 5% from its constant value in the dispersive regime (i.e., $R=0$ which is equal to the dimensionless width L' of the computational domain). In Fig. 9(a), it is shown that for $0<b<1$ the time of deviation of $I(t)$, from its value corresponding to $R=0$, increases with b. However, for $b>1$ an opposite scenario is observed, i.e., $I(t)$ starts deviating early with increasing b. The onset time calculated for different values of b from Fig. 9(a) is plotted in Fig. 9(b) as a function of b. It clearly shows onset time $t_{\rm vf}$ increases until $b=1$ [see inset Fig. 9(b)], but then again start decreasing. This change in trend of onset time of VF is because the spreading of the concentration due to advection rate decreases for large values of b. This aids in creating the steep concentration gradient which further results in early onset of VF for $b>1$. An important observation is that the onset time $t_{\rm vf}$ for $b>10$ is even below from the corresponding value for $b=0$. This observation is consistent, as for large values of b, we approach toward the no-adsorption case where onset of VF varies as $(1+k)$ times earlier than linear adsorption $b=0$ (cf. Mishra *et al.* [58]).

Thus, rarefaction wave can speed up or slow down the fingering instability, depending upon the adsorption parameter b. With a curve fitting done in MATLAB using "cftool," the

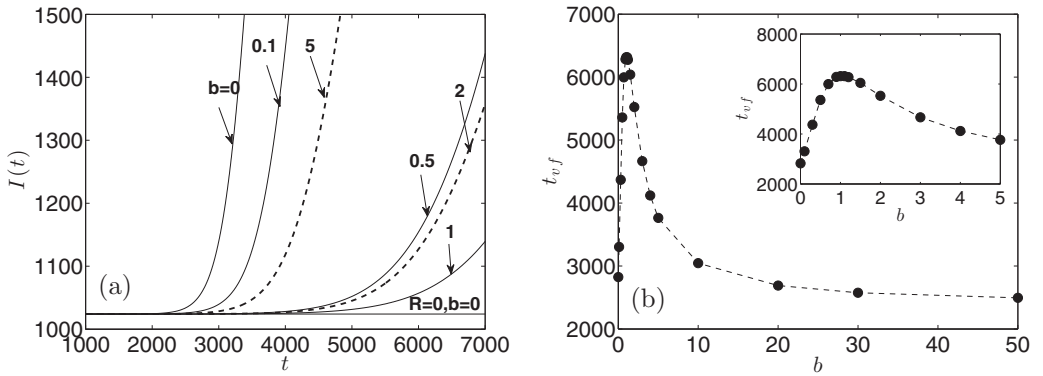

FIG. 9. (a) Temporal evolution of interfacial length, $I(t)$, with $R = 1,\ k = 0.2$ for different values of b and compared with the ideal case of stable displacement. (b) Onset time of VF, $t_{\rm vf}$, for different values of b with $R = 1,\ k = 0.2$. It shows a nonmonotonicity with respect to b. Inset: Zoomed in $t_{\rm vf}$ showing local maxima at $b \simeq 1$.

onset time of VF for different values of b with $R = 1,\ k = 0.2$ is found to follow Gaussian function having equation $a_1 b^{(1/1.3)}\exp(-b/2) + a_2$, where $a_1 = 1342,\ a_2 = 1076$. In the next section we discuss the influence of increase in log mobility ratio R on the onset time $t_{\rm vf}$ of viscous fingering.

D. Influence of log mobility ratio *R*

Here, the focus is to investigate the influence of log mobility ratio R on the fingering dynamics of the concentration. For that purpose, the concentration contours are plotted in Fig. 10(a) for different values of R with $b = 5,\ k = 0.2$ at a fixed time $t = 2000$. The concentration contours show that for $R = 1$, there are no fingers observed till this time. However, for larger values of R, the intense viscous fingering patterns are observed. The convective motion due to high mobility ratio, overtakes the rarefaction dynamics very early. Hence the rigorous fingering patterns are observed for $R = 2$ and 3. Further, we examine the influence of R on $t_{\rm vf}$ for different values of b. The onset time $t_{\rm vf}$ is calculated from interfacial length, the same way as that described in a previous Sec. IV C. The onset time $t_{\rm vf}$ is plotted in Fig. 10(b) as a function of b for different values of R. Clearly, irrespective of R, the onset time $t_{\rm vf}$ shows nonmonotonicity with a global maximum near $b = 1$. The most delayed onset is always in the vicinity of $b = 1$. The significant difference is observed in the variation in $t_{\rm vf}$ with b for different R. The variation of $t_{\rm vf}$ i.e., the difference between the onset time for most delayed and most early viscous fingering is decreasing with R. This can be clearly observed from visual comparison of the peak height of $t_{\rm vf}$ for $R = 1$ with $R = 2$ or 3. Thus, large variation in the onset time of viscous fingering is observed for $R = 1$ and this difference decreases with increasing R. We also observed that $t_{\rm vf}$ for very large values of b is lesser even from $b = 0$. In Fig. 10(b) the $t_{\rm vf}$ for $R = 3$ with $b = 10$ is lesser than the corresponding value with $b = 0$.

V. CONCLUSIONS

In this article the solute transport related to its adsorption on the porous medium is analyzed. Surface adsorption of solute has been widely studied, and this mechanism can be simplified using an isotherm equation which can be linear as well as nonlinear. The objective of this article was to analyze analytically and numerically, the displacement of miscible fluids with nonlinear adsorption of solute, where the initial concentration is a step-up profile. The analytical solution obtained by the method of characteristics for a unidirectional model

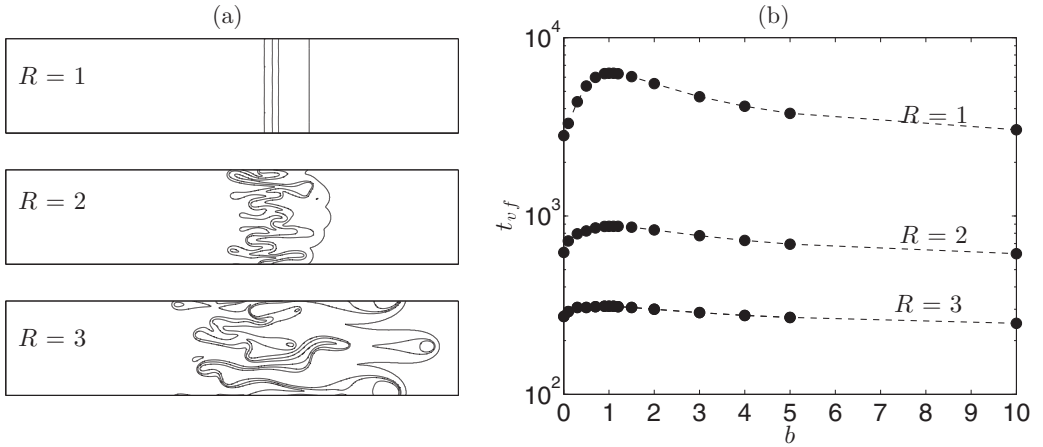

FIG. 10. (a) The concentration contour for different values of R, with $b = 5,\ k = 0.2$ at a fixed time $t = 2000$. The contour lines correspond to $c_m = 0.25,\ 0.5,\ 0.75$, and 1. (b) Onset time of viscous fingering $t_{\rm vf}$ as a function of b for different values of R with $k = 0.2$.

reveals the formation of rarefaction wave front as a result of hyperbolicity in the mass balance equation. To analyze the influence of the Langmuir adsorption in a stable as well as an unstable case, the set of governing equations in 2D are solved numerically using a Fourier-pseudo spectral method. It is found that for $R = 0$, the advection and dispersion rate being a function of the concentration c_m, results in the formation of nonsharpening waves which enhance the spreading. Thus, the spreading of the concentration increase with increase in b. However, it eventually decreases for large values of b, as the adsorption model approaches the no-adsorption case. Thus, it is concluded that the dynamics of the system are determined by the value of adsorption parameter b. Furthermore, it is shown that the flow development can be fully characterised by examining the influence of advection and dispersion rate on the transverse averaged concentration profiles.

The interesting dynamics are observed when there is viscosity contrast between the displacing fluid and the solute, along with the Langmuir adsorption of an initially step-up profile, giving rise to the interaction of VF and the rarefaction wave front to each other due to coupling between them. Such step-up concentration profile with the viscosity gradients solutions is very much useful for investigating the separation performance of high molecular weight protein samples, in polymer flooding or understanding the spreading of contaminants [17,42,55,60]. The analysis of the fingering dynamics with Langmuir adsorption, shows that the onset of instability in this semi-infinite domain, unlike to finite extent of the solute, is delayed for $b \lesssim 1$. Whereas, for $b > 1$ the onset time of VF start decreasing with b. This scenario is independent of the log mobility ratio R. However, for large values of b the onset time is observed to be earlier in comparison to $b = 0$. Thus, rarefaction wave can slow down or speed up the instability phenomena depending upon b. The spatiotemporal analysis shows the formation of lesser number of fingers in the Langmuir adsorbed solute. The merging is also reduced in comparison to linear adsorption along with disappearance of splitting phenomena for $R = 1$. These observations is different than the case studied in the literature when there is a finite extent of solute exist. Due to the finiteness of sample, the rarefaction wave can spread the sample to the left and the existence of shock layer from the frontal interface affects the VF dynamics of the rear interface. Since the log-mobility ratio reduces with time due to the finiteness, so the effect of such mobility ratio on the rarefaction wave cannot be the same as explained in this paper, in which no transient dynamics of the mobility ratio exist. The implication of these observations is that for practical purposes, rarefaction wave can be introduced to attain stability in a system for a long time which can be useful in the frontal analysis of chromatographic separation. The other interesting conclusion from this study is that the rarefaction wave formation with the most optimized adsorption parameter, means a mode of modifying the surface of porous matrix, can be an effective tool for controlling the VF dynamics.

APPENDIX: THE ANALYTIC RAREFACTION PROFILE

The unidimensional transport equation of the solute transport, with Langmuir adsorption isotherm and in the absence of diffusion is

$$\frac{\partial}{\partial t}\left(1 + \frac{k}{(1 + bc_m)}\right)c_m + \frac{\partial c_m}{\partial x} = 0. \tag{A1}$$

Equation (A1) can be simplified to obtain

$$\frac{\partial c_m}{\partial t} + f(c_m)\frac{\partial c_m}{\partial x} = 0, \tag{A2}$$

where $f(c_m) = \frac{(1+bc_m)^2}{k+(1+bc_m)^2}$. This is a first-order hyperbolic partial differential equation associated with the initial condition

$$c_m(x) = \begin{cases} 0, & \text{for } x < 0, \\ 1, & \text{for } x \geqslant 0. \end{cases} \tag{A3}$$

The family of characteristics for Eq. (A2) is given by

$$c_m = c_m(x_0), \tag{A4}$$

$$\text{where,} \quad x = x_0 + B(x_0)t, \tag{A5}$$

and $B(x_0) = f[c_m(x_0)]$. Since the slope of the characteristic is a function of concentration c_m, the concentration profile is propagating with a variable speed. For Langmuir adsorption

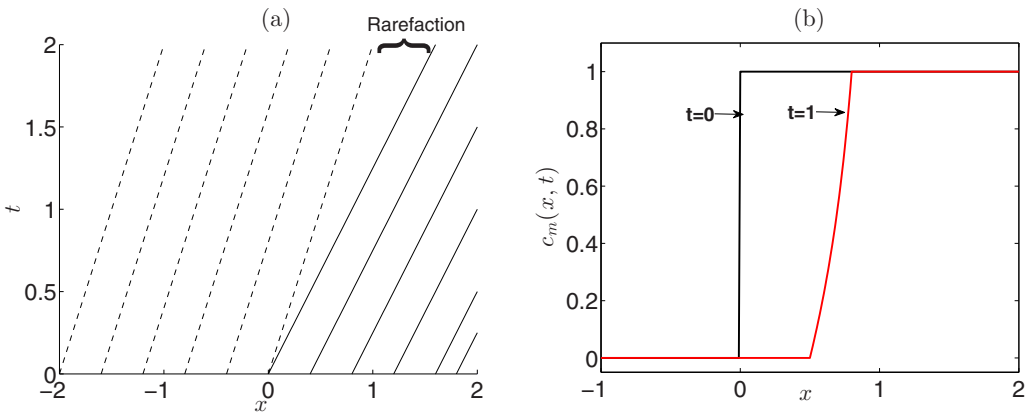

FIG. 11. (a) Characteristics showing formation of rarefaction wave for $k = 1$, $b = 1$. (b) The corresponding rarefaction wave solution of the concentration c_m at $t = 1$.

with $b > 0$ the slope of characteristics gives

$$\frac{dB}{dc_m} = \frac{2bk(1+bc_m)}{[k+(1+bc_m)^2]^2} > 0. \tag{A6}$$

This implies that slope of characteristics $B(c_m)$ is an increasing function of c_m. Hence, the higher concentration of c_m moves faster than lower concentration. Now with the initial condition of step-up profile [Eq. (A3)], expanding characteristics giving rise to a rarefaction wave are obtained. The corresponding characteristics obtained from Eq. (A4) are shown in Fig. 11(a) for $k = 1,\ b = 1$. Clearly, the characteristics are expanding and a rarefaction zone is formed.

The solution of Eq. (A2) is then given by

$$c_m(x,t) = \begin{cases} 0, & \text{for} \quad x/t < \frac{1}{(1+k)}, \\ \frac{(\frac{c_m}{1-c_m})^{1/2}-1}{b}, & \text{for} \quad \frac{1}{(1+k)} \leqslant x/t \leqslant \frac{(1+b)^2}{k+(1+b)^2}, \\ 1, & \text{for} \quad x/t > \frac{(1+b)^2}{k+(1+b)^2}. \end{cases}$$

This solution is plotted in Fig. 11(b) for $k = 1,\ b = 1$, showing the formation of nonsharpening wave. Occasionally, this solution is referred to as a rarefaction wave as it expands with time.

[1] W. Littmann, *Polymer flooding* (Elsevier, Amsterdam, 1988).
[2] L. M. Abriola, Rev. Geophys. **25**, 125 (1987).
[3] W. J. Weber Jr., P. M. McGinley, and L. E. Katz, Water Res. **25**, 499 (1991).
[4] B. Metz, O. Davidson, H. C. de Coninck, M. Loos, and L. A. Meyer, *IPCC Special Report on Carbon Dioxide Capture and Storage* (Cambridge University Press, New York, 2005).
[5] M. Sahimi, *Flow and Transport in Porous Media and Fractured Rock: From Classical Methods to Modern Approaches* (Wiley-VCH, Hoboken, NJ, 1995).
[6] G. Guiochon, A. Felinger, D. G. Shirazi, and A. M. Katti, *Fundamentals of Preparative and Nonlinear Chromatography* (Academic Press, San Diego, 2006).
[7] B. Berkowitz, A. Cortis, M. Dentz, and H. Scher, Rev. Geophys. **44**, RG2003 (2006).
[8] D. M. Ruthven, *Principles of Adsorption and Adsorption Processes* (Wiley, New York, 1984).
[9] S. Pramanik and M. Mishra, Chem. Eng. Sci. **122**, 523 (2015).
[10] T. Gérard and A. De Wit, Phys. Rev. E **79**, 016308 (2009).
[11] L. A. Riolfo, Y. Nagatsu, S. Iwata, R. Maes, P. M. J. Trevelyan, and A. De Wit, Phys. Rev. E **85**, 015304(R) (2012).
[12] F. G. Helfferich and P. W. Carr, J. Chromatogr. **629**, 97 (1993).
[13] P. H. Krumrine, J. S. Falcone Jr., and T. C. Campbell, Soc. Pet. Eng. **22**, 503 (1982).
[14] A. Sayari and Y. Belmabkhout, J. Am. Chem. Soc. **132**, 6312 (2010).
[15] C.-T. Hsu, C.-H. Chang, and S.-Y. Lin, Langmuir **13**, 6204 (1997).
[16] B. Berkowitz, I. Dror, and B. Yaron, *Contaminant Geochemistry* (Springer, Berlin, 2008).
[17] J. J. Sheng, *Modern Chemical Enhanced Oil Recovery: Theory and Practice* (Elsevier, Amsterdam, 2011).
[18] N. Ayawei, A. N. Ebelegi, and D. Wankasi, J. Chem. **2017**, 3039817 (2017).
[19] D. De Vault, J. Am. Chem. Soc. **65**, 532 (1943).
[20] L. Edström, J. Samuelsson, and T. Fornstedt, J. Chromatogr., A **1218**, 1966 (2011).
[21] J. G. Dominguez and G. P. Willhite, Soc. Pet. Eng. **17**, 111 (1977).
[22] C. Rana and M. Mishra, Phys. Fluids **29**, 032108 (2017).
[23] J. Zhu and G. Guiochon, J. Chromatogr. **636**, 189 (1993).
[24] J. Zhu, Z. Ma, and G. Guiochon, Biotechnol. Progr. **9**, 421 (1993).
[25] L. D. Plante, P. M. Romano, and E. J. Fernandez, Chem. Eng. Sci. **49**, 2229 (1994).
[26] H. Emami-Meybodi, H. Hassanzadeh, C. P. Green, and J. Ennis-King, Int. J. Greenhouse Gas Control **40**, 238 (2015), special Issue commemorating the 10th year anniversary of the publication of the Intergovernmental Panel on Climate Change Special Report on CO2 Capture and Storage.
[27] J. R. Boulding and J. S. Ginn, *Practical Handbook of Soil, Vadose Zone, and Ground-Water Contamination: Assessment, Prevention, and Remediation* (Lewis Publishers, Boca Raton, FL, 2004).
[28] P. G. Saffman, J. Fluid Mech. **173**, 73 (1986).
[29] G. M. Homsy, Annu. Rev. Fluid Mech. **19**, 271 (1987).
[30] M. L. Dickson, T. T. Norton, and E. J. Fernandez, AIChE **43**, 409 (1997).
[31] M. Mishra, M. Martin, and A. De Wit, Phys. Fluids **21**, 083101 (2009).
[32] M. Mishra, M. Martin, and A. De Wit, Chem. Eng. Sci. **65**, 2392 (2010).
[33] S. Keunchkarian, M. Reta, L. Romero, and C. Castells, J. Chromatogr. A **1119**, 20 (2006).
[34] C. Rana, A. De Wit, M. Martin, and M. Mishra, RSC Adv. **4**, 34369 (2014).
[35] T. K. Hota, S. Pramanik, and M. Mishra, Phys. Rev. E **92**, 023013 (2015).
[36] X. Zhou, M. Dong, and B. Maini, Fuel **108**, 261 (2013).
[37] C. G. Zheng, B. L. Gall, H. W. Gao, A. E. Miller, and R. S. Bryant, in *Proceedings of the SPE/DOE Improved Oil Recovery Symposium* (Tulsa, OK, 1998).
[38] S. Al-Hajri, S. M. Mahmood, H. Abdulelah, and S. Akbari, Energies **11**, 2751 (2018).
[39] R. Farazadeh, B. L. Wassing, and L. W. Lake, Energy Rep. **5**, 570 (2019).
[40] H. J. Catchpoole, R. A. Shalliker, G. R. Dennis, and G. Guiochon, J. Chromatogr. A **1117**, 137 (2006).
[41] S. R. Gallant, A. Kundu, and S. M. Cramer, J. Chromatogr. A **702**, 125 (1995).
[42] M. Enmark, D. Åsberg, A. Shalliker, J. Samuelsson, and T. Fornstedt, J. Chromatogr. A **1400**, 131 (2015).
[43] M. B. Allen III, G. A. Behie, and J. A. Trangenstein, *Multiphase Flow in Porous Media* (Springer-Verlag, Berlin, 1988).
[44] W. Lambert, D. Marchesin, and J. Bruining, Transp. Porous Media **81**, 505 (2010).

[45] J. Gruber, in *Sediments and Toxic Substances: Environmental Effects and Ecotoxity*, edited by W. Calmano and U. Förstner (Springer-Verlag, Berlin, 1996), Chap. 11, pp. 271–328.
[46] C. Rana, S. Pramanik, M. Martin, A. D. Wit, and M. Mishra, Phys. Rev. Fluids **4**, 104001 (2019).
[47] C. Rana, W. D. Malsche, and A. D. Wit, Chem. Eng. Sci. **203**, 415 (2019).
[48] T. T. Al-Housseiny, P. A. Tsai, and H. A. Stone, Nat. Phys. **8**, 747 (2012).
[49] N. Sabet, H. Hassanzadeh, and J. Abedi, Phys. Rev. E **96**, 063114 (2017).
[50] M. Mishra, M. Martin, and A. De Wit, Phys. Rev. E **78**, 066306 (2008).
[51] C. Canuto, M. Y. Hussaini, A. Quarteroni, and T. A. Zang, *Spectral Methods in Fluid Dynamics* (Springer-Verlag, Berlin, 1988).
[52] C. T. Tan and G. M. Homsy, Phys. Fluids **31**, 1330 (1988).
[53] A. Rogerson and E. Meiburg, Phys. Fluids A **5**, 2644 (1993).
[54] H. Wei, L. Han, Y. Tang, J. Ren, Z. Zhao, and L. Jia, J. Mater. Chem. B **3**, 1646 (2015).
[55] M. Ali and H. B. Mahmud, in *IOP Conference Series: Materials Science and Engineering*, Vol. 78 (IOP Publishing, Bristol, UK, 2015), p. 012038.
[56] O. Falode and F. A. Afolabi, Pet. Coal **53**, 206 (2011).
[57] A. De Wit, Y. Bertho, and M. Martin, Phys. Fluids **17**, 054114 (2005).
[58] M. Mishra, M. Martin, and A. De Wit, Phys. Fluids **19**, 073101 (2007).
[59] C.-Y. Chen and S.-W. Wang, Int. J. Numer. Methods Heat Fluid Flow **11**, 761 (2001).
[60] R. Vishnudas and A. Chaudhuri, Fuel **194**, 480 (2017).